

4 Surface Tension Driven Instabilities

Surface tension plays an important role in localized melting processes such as welding and direct SLS. For instance, it is well known that the surface tension of pure metals is a decreasing function of temperature. Therefore, temperature gradients in a melt pool can give rise to surface tension gradients and associated Marangoni convection. It is also well known that small amounts of impurity elements can drastically alter the surface tension values and surface tension gradients, changing the direction of flow in the melt pool. Even under isothermal conditions, capillary instabilities are known to occur in the flow of jets, rivulets and planar bodies of fluids. These instabilities result from disturbances giving rise to surface waves whose amplitude can get large enough so that the fluid breaks up into smaller volumes to minimize surface free energy. Two aspects of surface tension driven effects influenced by the scan speed and scan spacing in SLS are addressed with their implications on the geometry of the laser processed and subsequently solidified melt.

To investigate the effect of scan speed on the shape of the solidified melt, single line scan experiments were performed by scanning 0.5 inch long lines on Alloy 625 powder at 80 Watts Nd:YAG laser powder, under high vacuum ($< 10^{-5}$ Torr) and without powder preheat (powder at ambient temperature). The flow and solidification behavior of the melt was captured by video microscopy at 30 frames/s. Testing at a variety of scan speeds confirmed that the flow behavior of the melt was very similar to the jet instability. At high scan speeds, the melt tended to be broken up or “atomized” into a number of droplets, whereas at slower scan speeds, the melted line tended to form regularly spaced beads or undulations whose size grew with decreasing scan speed, eventually tending towards jet break-up at very slow speeds. Figure 1 shows three scan lines Alloy 625. From left to right, the lines were scanned at 1.4 in/s, 0.7 in/s and 0.35 in/s respectively, showing the relative differences in line width, bead geometry and bead frequency as a function of scan speed.

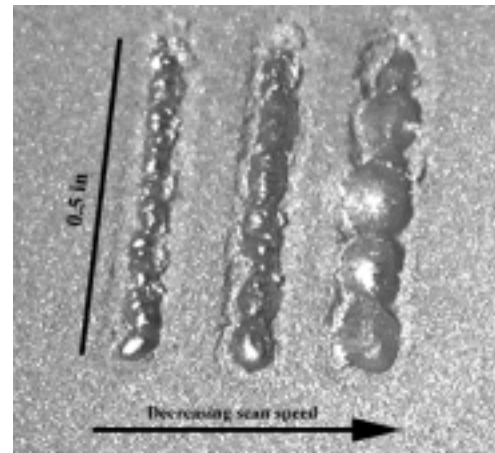


Figure 1: Single line scans on Alloy 625 at 1.4, 0.7 and 0.35 in/s.

Two types of instabilities were observed during raster scanning in SLS of metals. The first type, termed the starting edge instability occurs at the edge where raster scanning is

initiated. The molten material at the starting edge exhibits a tendency to break up or tear into smaller pieces. Under a wide variety of laser processing conditions, the tendency of the melt to break up was noted to attenuate after the first four or 5 lines were scanned. The flow behavior of the starting edge instability is very similar to the behavior of single line scans illustrated in the previous section. The second instability, termed surface instability, pertains to the formation of ripples on the surface of a solidified layer. At fixed laser power, scan speed and scan vector length, this instability is strongly attenuated by decreasing the scan spacing.

Single layer raster scan experiments were performed by scanning 0.5 inch long lines at 11.2 in/s on Alloy 625 powder (-325 mesh) at 80 Watts Nd:YAG laser powder, under high vacuum ($< 10^{-5}$ Torr) and without preheating the powder. The flow and solidification behavior of the melt was captured by video microscopy at 30 frames/s. Testing at a variety of scan spacings confirmed that the flow and solidification behavior of the melt was very strongly influenced by the scan spacing. A progressive transition from a highly rippled surface to a very smooth surface occurs with decreasing scan spacing.

Shown in Figure 2 are selected video frames of a single layer raster scanned at 0.005 inches scan spacing. The tendency of the melt produced by the first scanned line to break up is apparent in frame 1. Frame 2 reveals that with progressive scanning, the break at the middle of the starting edge stabilizes and does not propagate. However, the starting edge attains a highly irregular definition, while the trailing edge is well defined. Frame 3 shows the poor surface finish of the entire layer.

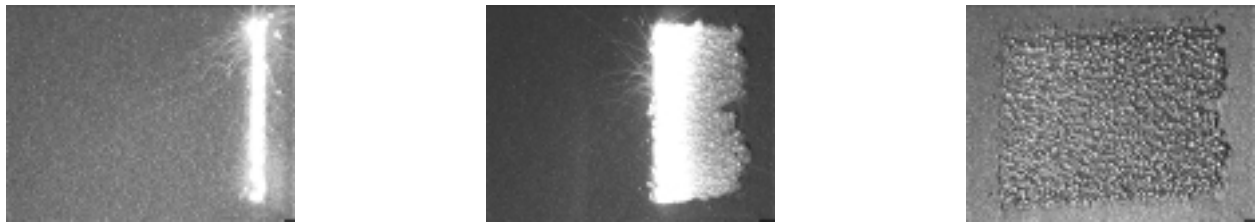


Figure 2: A layer of Alloy 625 scanned at 0.005 inches scan spacing

A raster scan spacing of 0.0005 inches is about the smallest scan spacing available on the scanning apparatus used for these experiments. By inspecting layers scanned with scan spacings ranging from 0.005 to 0.0005 inches, it was clear that while the starting edge instability manifests itself across all cases, as scan spacing decreases, the surface instabilities are damped out resulting in progressively smoother solidified surfaces. The starting edge instability is associated with the short interaction time of the moving laser beam with the powder, causing it to locally melt coupled with the inherent tendency of a liquid stream to break up into smaller pieces. In raster scanning mode, if the time for the laser beam to return to a previously scanned location is longer than the local solidification time, then that portion of the layer has already solidified and possibly substantially cooled below the melt temperature. It has been observed experimentally that the laser beam operating in continuous wave (CW) mode is typically unable to substantially remelt the solidified material. The scan spacings used in the above cases were all smaller than the laser beam diameter (of order 0.020 inches). Therefore, during raster scanning, each point on the scanned surface was

overlapped multiple times by the laser beam, the degree of overlap increasing with decreasing scan spacing.

To qualitatively understand the effect of scan spacing on the temperature history, constant vector length raster scanning can be idealized as an infinite medium moving at a constant speed U past a strip heat source of fixed width equal to the beam diameter at the scan plane. Only pure conduction is considered in this analysis. In SLS, if the scan vector length is l and the scanning speed of the rastering laser beam is v , then the time taken to scan one vector is t_v given by

$$t_v = \frac{l}{v}$$

After scanning a vector, the laser beam is indexed over to the starting position of the next vector by a distance equal to the scan spacing δ . This movement takes place very rapidly and hence the time taken to index the beam is negligible compared to t_v . Therefore, we can assume for all intents and purposes that the total time to index the beam by a distance δ in the transverse direction is t_v . Therefore, the transverse velocity of the idealized moving line source is given by

$$U = \frac{\delta}{t_v}$$

It is readily apparent that for a fixed scanning speed v and fixed scan vector length l (as was maintained in the experiments described above), The transverse speed U is directly proportional to the scan spacing δ . If Q is the heat emitted per unit time per unit area over the strip, the steady state temperature distribution at a point (x, y, z) in the medium for a infinite strip source $-b < x < b$, $-\infty < y < \infty$ in the plane $z = 0$ is given by [1]

$$T(x, y, z) = \frac{Q}{2\pi K} \int_{-b}^b e^{-U(x-x')/2\kappa} K_0 \left\{ U[(x-x')^2 + z^2]^{1/2} / 2\kappa \right\} dx' \quad (1)$$

where K is the thermal conductivity, κ is the thermal diffusivity and K_0 is the modified Bessel function of the second kind of order 0. By defining the dimensionless variables

$$X = \frac{Ux}{2\kappa}, \quad Z = \frac{Uz}{2\kappa}, \quad B = \frac{Ub}{2\kappa} \quad (2)$$

the integral of equation 1 at the surface ($z=0$) becomes

$$T(x, y, 0) = \frac{\kappa Q}{\pi K U} \int_{X-B}^{X+B} e^{-u} K_0 \{|u|\} du \quad (3)$$

The generic form of the integral in equation 3 is given by [2]

$$\begin{aligned} I(a) &= \int_0^a e^{-u} K_0 \{|u|\} du = ae^{-a} \{K_0(a) - K_1(a)\} + 1, \quad a > 0 \\ &= -\int_0^a e^u K_0 \{|u|\} du = 1 - ae^a \{K_0(a) + K_1(a)\}, \quad a < 0 \end{aligned} \quad (4)$$

where K_0 is as defined before and K_1 is the modified Bessel function of the second kind of order 1.

Therefore, equation 3 can be rewritten as

$$T(x, y, 0) = \frac{\kappa Q}{\pi K U} [I(X + B) - I(X - B)] \quad (5)$$

Plots of the steady-state temperature (scaled by $\frac{\pi K}{\kappa Q}$) as a function of strip source location x (scaled by $\frac{1}{b}$) for various values of δ are shown in Figure 3, with each successive value of δ half the previous value, as was selected in the experiments. The instantaneous location of the strip heat source center line is at $x = 0$. As expected, from the plots of Figure 3, it is apparent that the steady state temperature is inversely proportional to scan spacing. Therefore, in the real situation where melting and solidification are taking place in addition to heat conduction, it is expected that scanned regions will remain at higher temperatures for longer times. Thus, it is conceivable that under certain conditions of laser power and scan speed, as scan spacing is decreased, local regions could remain molten (or in the mushy state) during successive passes of the laser (i.e. for a number of contiguous vectors). Thus, increasing the solidification time for a strip like region parallel to the direction of the scanning laser beam, while maintaining uniformity of temperature along its scan length could allow for surface tension driven instabilities in the melt to be damped out, resulting in improved surface flatness or smoothness, as observed experimentally.

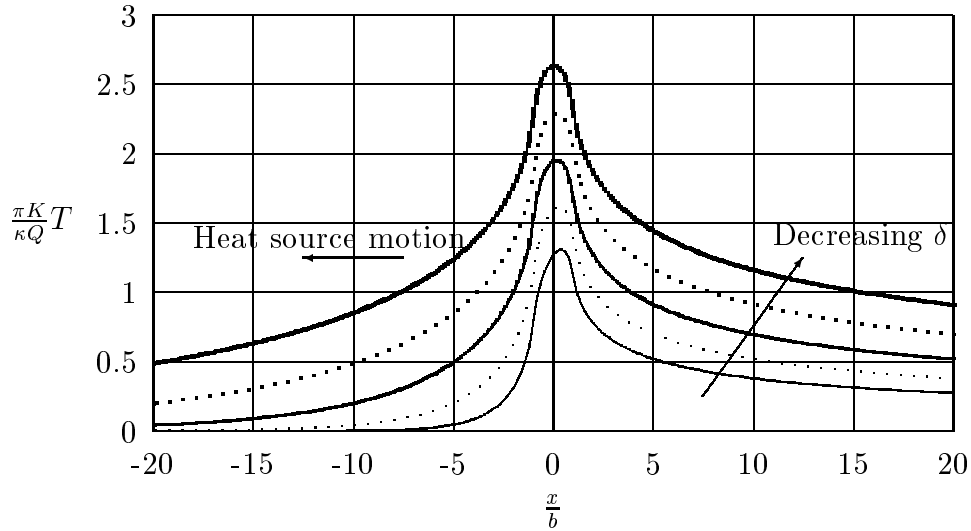


Figure 3: Steady state temperature vs. coordinate for a strip heat source.

One method of eliminating the starting edge instability is to displace the starting edge into the interior of the layer while minimizing the length of the starting scan vectors. In the extreme case, the starting scan vector can be reduced to a point. This technique can be easily applied by starting the scan at the center and tracing concentric patterns of increasing dimension towards the edges. An example of this technique for a circular cross-section is

shown in Figure 4. In this case, the laser starts at the center of the circle and traces an Archimedean spiral. As can be seen in frames 1, there is no balling or beading of the melted and resolidified material. Frames 2 and 3 show not only a flat solidified layer surface but also excellent edge definition at the outward propagating solidification front. In addition to eliminating the starting edge instability, with the absence of abrupt changes in scan direction, this type of scanning ensures that continuity of the solid-liquid interface is maintained at the instantaneous location of the moving laser beam. Maintaining continuity of the moving solid-liquid interface is essential to avoid macro-porosity and other defects in materials processed by direct SLS.



Figure 4: Archimedes spiral, scanned at 0.00125 inches scan spacing

5 Powder Caking

Powder bed caking has been observed while preheating powder during SLS processing. For Alloy 625 and Ti-6Al-4V, 450° C and 350° C respectively were the threshold preheat temperatures at which substantial powder caking was noted to occur. It was also noted that despite Ti-6Al-4V having a 250° C higher melting temperature range and twice the particle size as that of Alloy 625, its tendency was to cake more vigorously. Therefore, a study was undertaken to understand the low temperature (with respect to melting temperature) sintering characteristics of metal powder materials and their effects on powder morphology.

Powder caking is the result of sintering (necking and densification) between adjacent powder particles. Sintering is initiated by thermally activated mass transport between powder particles and is typically observed to consist of three stages, namely initial stage sintering, intermediate stage sintering and final stage sintering.

During initial stage sintering, surface transport and bulk transport are the primary modes of mass transport contributing to necking and densification. In surface transport, surface diffusion and evaporation-condensation are the two most significant mechanisms, while for bulk transport volume diffusion, grain boundary diffusion, plastic flow and viscous flow are the most significant. The distinction between the two primary modes is that surface transport leads to neck formation and neck growth without net volume change (*i.e.* densification), whereas bulk transport results in shrinkage.

German [3] states that surface diffusion dominates low temperature sintering in many metals. For bulk transport, he states that plastic flow is important for sintering of compacted powders with high dislocation density while viscous flow must be considered when a liquid phase appears at the grain boundaries. It is also stated that grain boundary diffusion is quite

important in the densification of most crystalline materials. In view of the above arguments, only surface diffusion, volume diffusion and grain boundary diffusion were considered for the investigation of low temperature sintering to explain the caking behavior of loosely packed preheated powders in SLS.

To study powder caking as a result of powder preheat in SLS, we restrict ourselves to initial stage sintering. The general equation for initial stage sintering (final fractional density < 70%) is given by [3]

$$\left(\frac{X}{D}\right)^n = \frac{Bt}{D^m} \quad (6)$$

where X is the neck diameter, D is the powder particle diameter, B is a parameter governed by the dominant sintering mechanisms, t is the time and the exponents n and m are also determined by the specific sintering mechanisms. Equation 6 is generally valid for the range $0 \leq \frac{X}{D} \leq 0.3$. The form of the parameter B and its dependence on material properties for each of these mechanisms is listed by German [3]. The forms of the parameters B , m and n for volume diffusion, grain boundary diffusion and surface diffusion are shown in Table 1, where γ is the surface energy, D_v , D_b and D_s are the temperature dependent (Arrhenius form) diffusion constants for volume, grain boundary and surface diffusion respectively, Ω is the atomic volume, δ is the grain boundary width, k is Boltzmann's constant and T is the temperature.

Mechanism	n	m	B
Lattice (volume) diffusion	5	3	$80D_v\gamma\Omega/(kT)$
Grain boundary diffusion	6	4	$20\delta D_b\gamma\Omega/(kT)$
Surface diffusion	7	4	$56D_s\gamma\Omega^{4/3}/(kT)$

Table 1: Sintering parameters for volume, grain boundary and surface diffusion.

Initial stage sintering curves incorporating the cumulative effect of mechanisms in Table 1 for titanium (α and β), nickel, MARM200 (a nickel base superalloy) and stainless steel 304L are shown in Figure 5 for 300° C. Several sintering characteristics are readily discernible from these graphs. At the same particle size and temperature, the alloys (MARM200 and SS304L) show lesser sintering activity than the pure elements. At 300° C and 0.5 hours, the neck radius exceeds 5% and 2% of the particle diameter for the pure elements and the alloys respectively. At 450° C at 0.5 hours, the neck radius for pure elements is more than about 18% of the particle diameter for the elements and approaching 10% for the alloys. The sintering activity rises dramatically at 600° C such that at 0.1 hours, the sintering curves for the elements are out of the range of validity of equation 6.

These results explain the caking behavior as a result of preheat observed for Alloy 625 and Ti-6Al-4V. It is expected that the caking behavior of Alloy 625 (a nickel base superalloy) will be similar to that of MARM200 while the caking behavior of Ti-6Al-4V (an $\alpha - \beta$ alloy) will lie between that of α titanium and β titanium. Powder caking due to preheat is highly undesirable in SLS. For successful delivery and laser consolidation of powder layers, it is vitally important to maintain free flowing characteristics of the feedstock powder. The initial stage isothermal sintering model predicts that significant inter-particle necking and

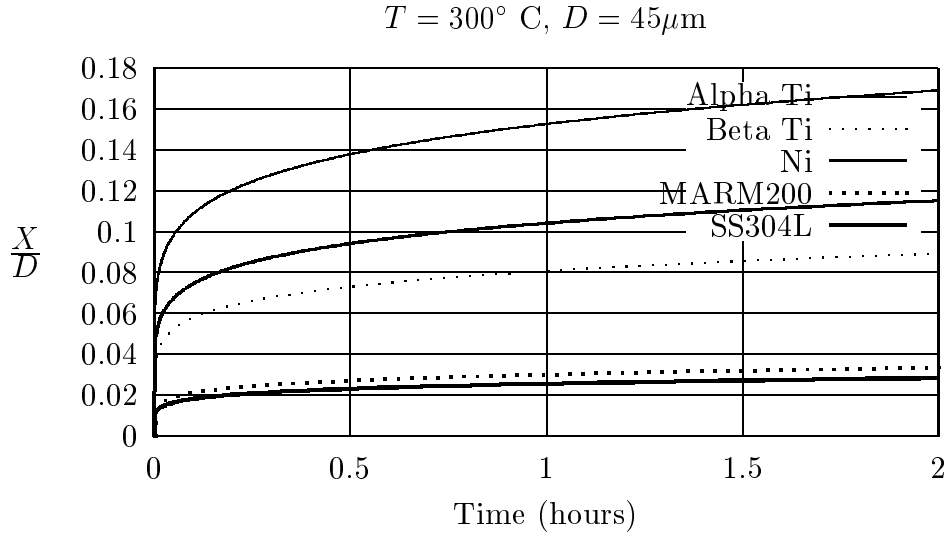


Figure 5: Neck diameter vs. time at 300° C.

associated powder caking will occur at preheat temperatures as low as 300° C. Therefore, preheat at lower temperatures (100° C to 200° C) could be used for *in situ* dynamic degassing of adsorbed contaminants from feedstock powder while being able to avoid caking. However, tremendous cost benefits are achievable by eliminating the need for a heating system in a SLS machine. The ability to fabricate full density components by SLS without any external powder bed preheat has been demonstrated for Ti-6Al-4V [?] and is expected for other materials as well. A heaterless SLS machine for metals will require having an off-line powder degas apparatus with appropriate “clean handling” procedures to transfer degassed powder to the SLS chamber without contamination or exposure to air. The advantages of having such a combination far outweigh the advantages of having an integral low temperature heating system in the HTW.

6 Conclusions

An understanding of some of the important physical mechanisms in SLS processing of metals was achieved. This understanding is crucial to machine design and process control development. The following conclusions can be made with respect to successful direct SLS processing of metals.

1. Processing atmosphere control using high vacuum or low oxygen partial pressure ultra-pure environment is necessary to prevent surface contamination, poor wetting and internal oxidation.
2. Poor wetting can occur even with good atmosphere control. The mechanism for “good wetting” in direct SLS of metals is epitaxial solidification by heterogeneous nucleation.

In order to obtain full density, partially remelting previously formed, underlying layers is necessary to induce epitaxial solidification.

3. SLS processing under vacuum results in volatilization of alloying elements to due reduction of vaporization temperatures. Volatilization and subsequent condensation on the laser window causes inconsistent laser energy delivery while condensation on chamber internal surfaces can potentially contaminate other materials processed subsequently. Partial pressure processing with a continuous flow of ultra-pure inert gas increases the vaporization temperature, reduces the mean free path, alleviates elemental volatilization and flushes away volatilized material from the processing zone.
4. Surface tension driven instabilities in raster scanning occur at the starting edge and on the processed surface. In raster scanning, the starting edge instability persists while surface instabilities are alleviated by using a fine scan spacing. Both instabilities can be eliminated by starting the scan at a point and progressing outward in a continuous path to fill the area to be consolidated.
5. Preheating metal powders at low to moderate temperatures leads to solid state sintering, caking and poor powder flow. Preheating and associated caking are detrimental to SLS processing and are not recommended.

References

- [1] H. S. Carslaw and J. C. Jaeger. *Conduction of Heat in Solids*, chapter X, page 267. Oxford University Press, Inc., 1959.
- [2] J. C. Jaeger. Moving Sources of Heat and Temperature at Sliding Contacts. *Proceedings of the Royal Society of New South Wales*, 76:203–224, 1943.
- [3] Randall M. German. *Powder Metallurgy Science*, chapter 7. MPIF, 1994.